Supporting Information

Constructing dual-redox polyimides for enhanced hybrid capacitive deionization performance

Yuquan Li[a], Qingyu Hong[a], Qianrong Wang[a], Zehua Bian[a], Weiqi Fu[a], Can Ding[a], Likun Pan[b]*, Xiaozhi Wang[a]*

[a] College of Environmental Science and Engineering, Yangzhou University, 196 West Huayang Road, Yangzhou 225091, China.

[b] Shanghai Key Laboratory of Magnetic Resonance, School of Physics, Institute of Magnetic Resonance and Molecular Imaging in Medicine, East China Normal University, Shanghai 200241, China.

Materials

N-methyl-2-pyrrolidinone (NMP), 2,6-Diaminoanthraquinone (DAAQ), p-Phenylenediamine (PPD), 1,4,5,8-naphthalene tetracarboxylic dianhydride (NTCDA), pyromellitic dianhydride (PMDA), ethanol, N, N-dimethylformamide (DMF), NaCl, and were purchased from Sinopharm Chemical Reagent Co., Ltd. The IEMs (Neosepta AMX membranes) are purchased from Tokuyama Corp., Japan. Polyvinylidene fluoride (PVDF), activated carbon (AC), and carbon black were purchased from Hefei Kejing Material Technology Co., Ltd. (China). Except AC, all reagents were used as received. Before used as electrode material. The AC was pre-treated with 0.5 M HCl overnight to remove residual salt ions, and heated at 280 ºC for 10 h in N_2 atmosphere.

Experimental Section

Synthesis of three polyimides: The synthesis of PI-1, PI-2, PI-3 were conducted according to a procedure reported by Zhang et al[1] (as shown in Figure S1). Briefly, 3 mmol DAAQ/ PPD was first dissolved in 60ml NMP, respectively. Equal molar ratio of NTCDA/ PMDA were then added to the above solution, respectively. The mixed solution stirred 30 min in an N_2 atmosphere. Then the mixed solution was transferred to a 100ml Teflon-lined stainless steel autoclave and maintained at 210℃ for 24h. After cooling down completely, the solid product was separated from the mixture and washed with deionized water and ethanol several times. The final product was Soxhlet extracted using DMF for 36 h to remove the soluble reactants and oligomer.

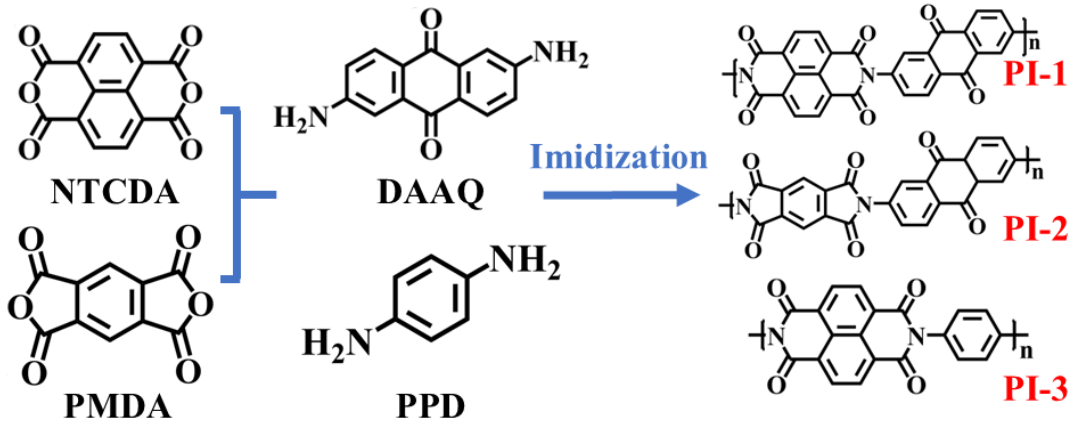

Fig. S1 Synthetic routes for PI-1, PI-2, PI-3.

Material characterization

The surface morphology and structure of samples were examined by field emission scanning electron microscopy (FESEM, JEOL JSM-LV5610). To study the bond structure of polyimides, the as-prepared polymer was characterized by Fourier transform infrared (FTIR) spectroscopy. Thermal gravimetric analysis (TGA) was conducted on a Shimadzu-50 themoanalyser in N_2 with a heating rate of 10 °C min^{-1} from room temperature to 800 °C. N_2 adsorption/desorption isotherms were measured using an ASAP 2020 Accelerated Surface Area and Porosimetry System (Micrometeritics, Norcross, GA) at 77 K. The specific surface areas of samples were estimated based on the Brunauer-Emmett-Teller (BET) model by using the adsorption branch data in the relative pressure (P/P0) range of 0.05-0.3.

Theoretical calculations

All calculations were performed using density functional theory (DFT) as implemented in the Gaussian 16 software package[2]. The HOMO-LUMO energies were computed with the 6-311G(d) basis set to ensure accuracy. Structural

optimizations for PI-1, PI-2 and PI-3 were conducted at the B3LYP/def2-SVP level of theory, yielding both optimized geometries and corresponding vibrational frequencies. Additionally, electrostatic potential (ESP) was conducted using Multiwfn 3.8 (dev) and visualized with VMD[3, 4]. The ESP image can be derived by solving the Poisson equation for the charge distribution and projected onto the molecular surface, with red and blue regions indicating electron rich (negative ESP) and electron-deficient (positive ESP) areas, respectively.

Electrode preparation

To prepare polyimide-based electrodes for desalination test, 80 mg polyimide was thoroughly mixed with 40 mg carbon black and 13.3 mg PVDF (in a 6: 3: 1 weight ratio) in NMP. The resulting slurry was coated onto a graphite paper (32 cm^2) and dried at 120 ºC in a vacuum drying oven overnight. The AC-based electrodes were prepared by adjusting the mass of AC, carbon black, and PVDF to 200, 25, and 25 mg (in a weight ratio of 8: 1: 1), respectively. The working electrodes for electrochemical measurements were prepared by a similar procedure, but on a smaller graphite paper (4 cm^2).

Electrochemical measurements

Cyclic voltammetry (CV, tested within 0~0.8 vs. Ag/AgCl electrode potential), galvanostatic charge-discharge (GCD, tested within -0.1~-0.9 vs. Ag/AgCl electrode potential for polyimide-based electrodes) tests were carried out on an electrochemical workstation (DH 7000D, Donghua Analytical) under deair condition in a three-

electrode mode, including an Ag-AgCl (in saturated KCl solution) electrode as reference electrode and a platinum foil as counter electrode.

Specific capacity (mAh g^{-1}) was calculated from GCD curves according to the following equation:

$$Specific\ capacity = \frac{I \times \Delta t}{m \times 3.6} \quad \text{(S1)}$$

where I is the current (A), Δt is the discharging time (s), m is the mass of active materials (g). In theory, the voltammetric response follows a power-law relationship of measured current with the scan rate according to the following equation:

$$i = av^b \quad \text{(S2)}$$

where i is the measured peak current (A), v is the scan rates (mV s^{-1}), and both a and b are adjustable parameters. For a typical intercalation process which is limited by a semi-infinite linear diffusion process, the peak current i varies with $v^{1/2}$ (b = 0.5); for a surface-controlled process, such as adsorption, it varies with v (b = 1).

Coulombic efficiency was calculated according to the following equation:

$$Coulombic\ efficiency = \int \frac{I_{cathodic} \times dt_{cathodic}}{I_{anodic} \times dt_{anodic}} \quad \text{(S3)}$$

Where $I_{cathodic}$ and I_{anodic} (A) are transient currents during dis-charge and charge processe.

Batch-mode electrosorption tests

The capacitive deionization (CDI) was constructed using an as-prepared polyimide-based electrode and an AC-based electrode. The desalination tests were conducted in a batch-type CDI testing setup under deair condition, as detailed in our earlier research.[5]. In brief, 80 mL of the 20 mM NaCl solution was continuously circulated

by a peristaltic pump (with a flow rate of 25 mL min^{-1}) through the CDI device and back to a water tank, where a conductivity sensor was installed. The conductivity of the solution was measured by a conductivity meter (DDS-308, Shanghai Precision & Scientific Instrument Co., Ltd.) every 60 s. The concentration of the NaCl solution was then determined from the calibration chart obtained before the experiment, according to a calibration table made prior to the experiment.[5] The concentrations of various cations during desalination processes were quantified via inductively coupled plasma optical emission spectrometer (ICP-OES, Agilent 5800). Salt adsorption capacity (SAC) (mg g^{-1}) was calculated as the following[6]:

$$SAC = \frac{(C_f - C_0) \times V}{M}$$

where C_f and C_0 are final and initial NaCl concentrations (mg L^{-1}), V is the solution volume (L) and M is total mass of electrodes (g). The charge efficiency (Λ) is used to determine the effectiveness of electrical double layer on storing salt ions and given as[7]:

$$\Lambda = \frac{SAC \times F}{58.44 \times 1000 \times \Sigma}$$

where Σ is specific charge (C g^{-1}) and F is the Faraday's constant of 96485 (C mol^{-1}). Na^+ removal capacity (mg g^{-1}) was calculated as the following:

$$Na^+ \ removal \ capacity = \frac{(C_f - C_0) \times V \times M_{Na} \div M_{NaCl}}{M_{cathode}}$$

where M_{Na} and M_{NaCl} are Molar masses of sodium and sodium chloride (g mol^{-1}), respectively, $M_{cathode}$ is mass of PI-based cathodes (g). Theoretical capacity (mAh g^{-1}) was calculated as the following:

$$Theoretical \ capacity = \frac{F \times n}{M_{repeat \ unit} \times 3.6}$$

where F is the Faraday's constant of 96485 (C mol^{-1}), n is the number of electrons transferred per repeat unit, and $M_{repeat\ unit}$ is the molar mass of the repeat unit. The Active site utilization rate was calculated as the following:

$$Active\ site\ utilization\ rate = \frac{Experimental\ capacity}{Theoretical\ capacity}$$

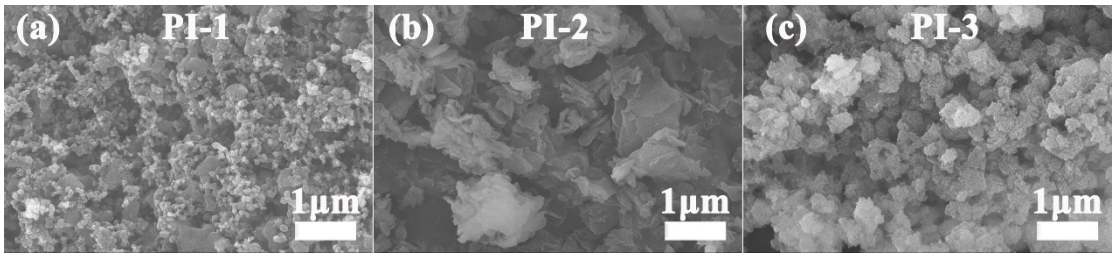

Fig. S2 FESEM images of PI-1, PI-2, PI-3.

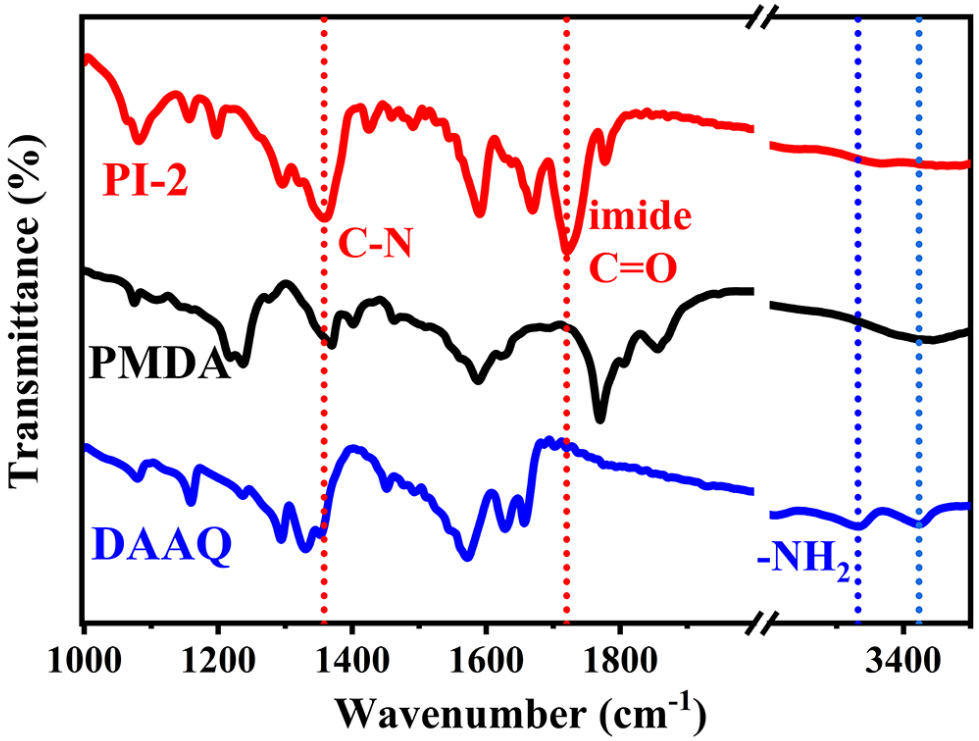

Fig. S3 FTIR spectrum for PI-2 and its precursor.

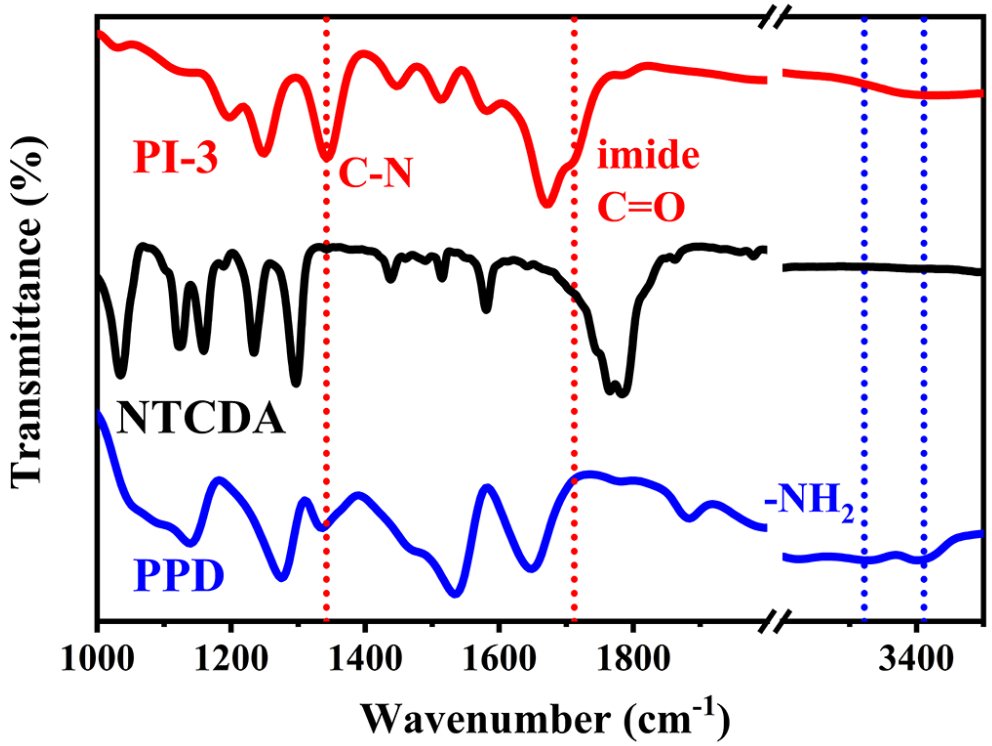

Fig. S4 FTIR spectrum for PI-3 and its precursor.

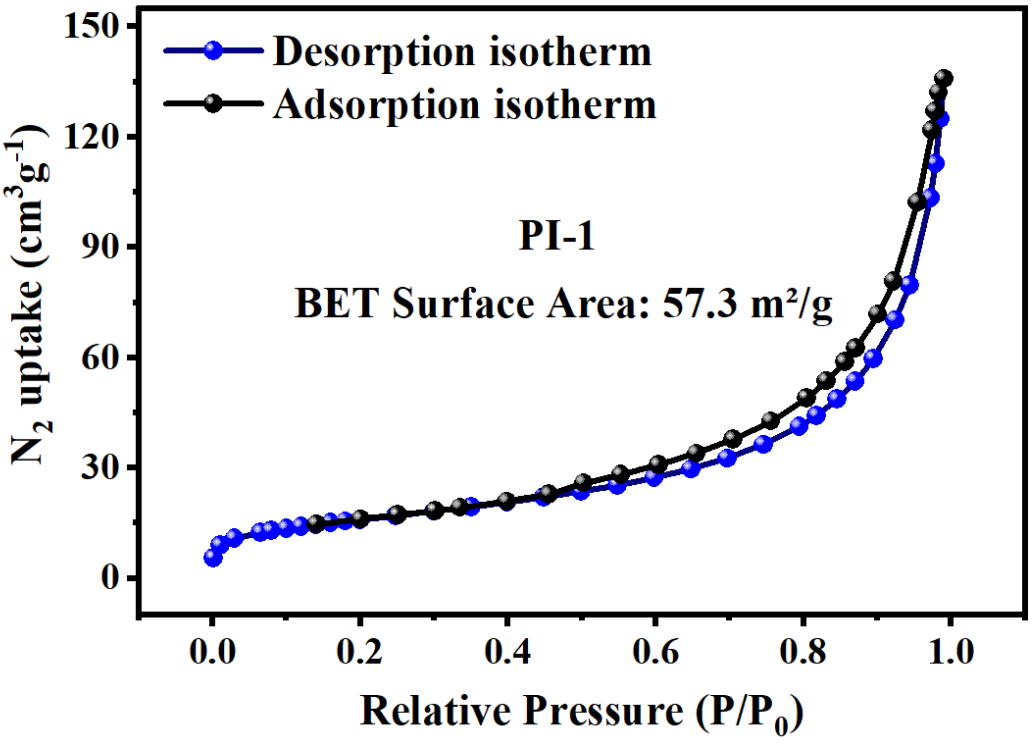

Fig. S5 N_2 adsorption–desorption isotherms for PI-1.

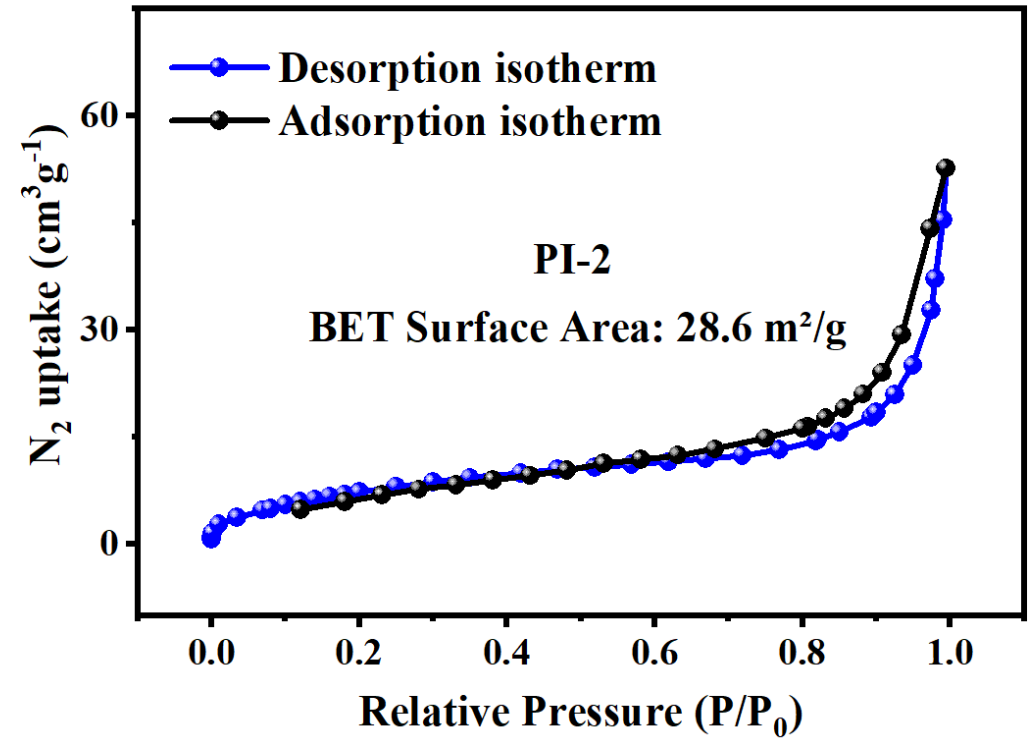

Fig. S6 N_2 adsorption–desorption isotherms for PI-2.

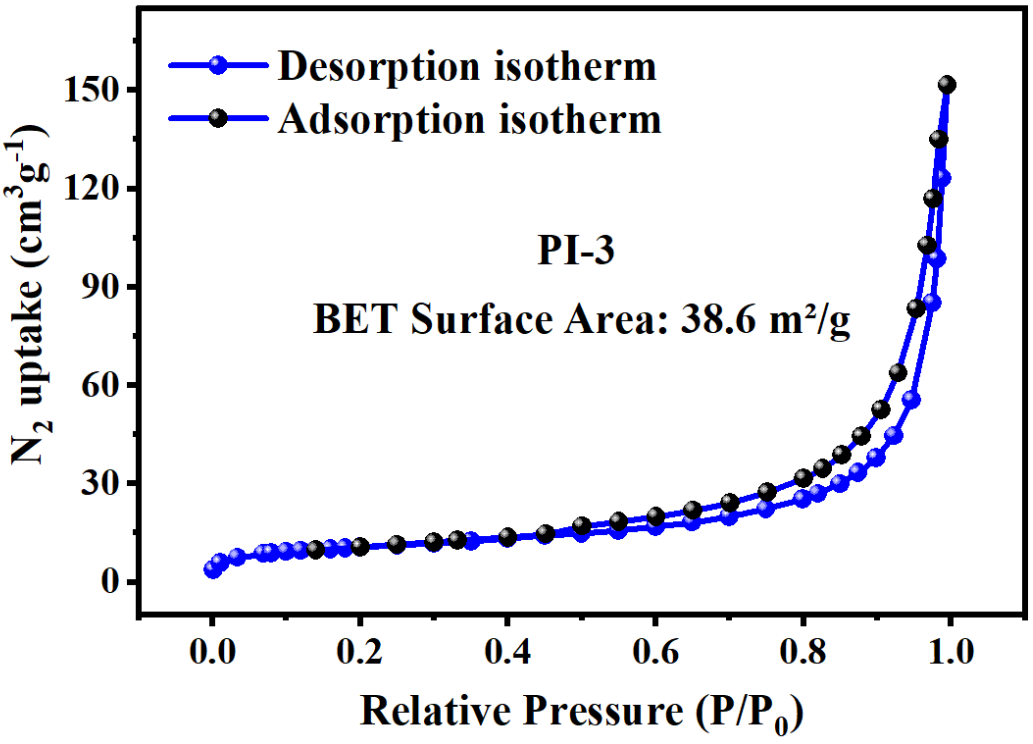

Fig. S7 N_2 adsorption–desorption isotherms for PI-3.

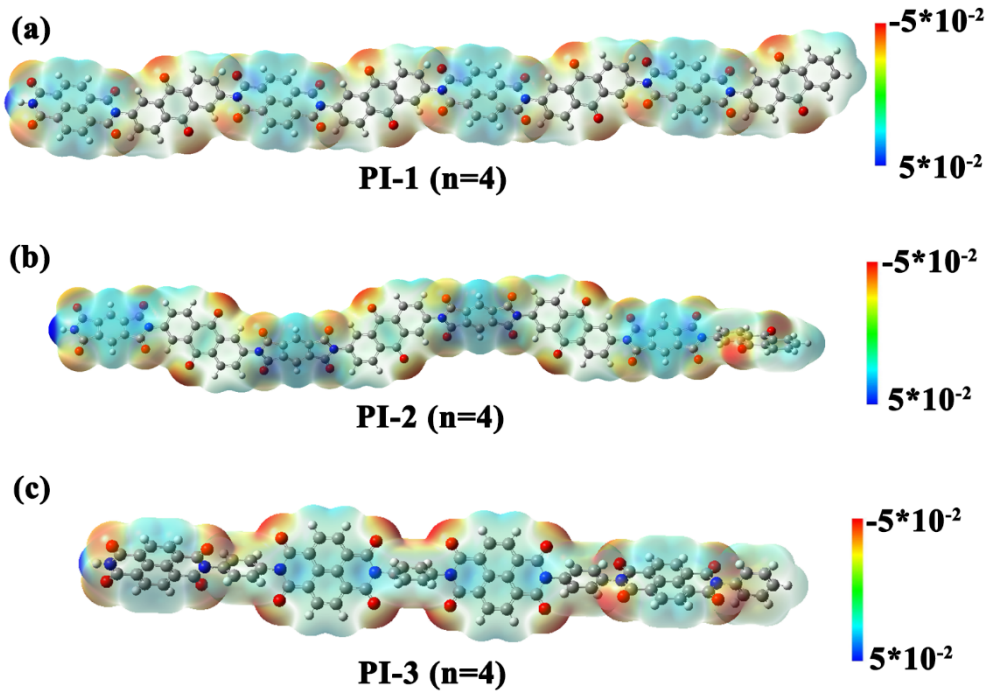

Fig. S8 Electrostatic potential surface map of PI-1, PI-2, PI-3 (n=4).

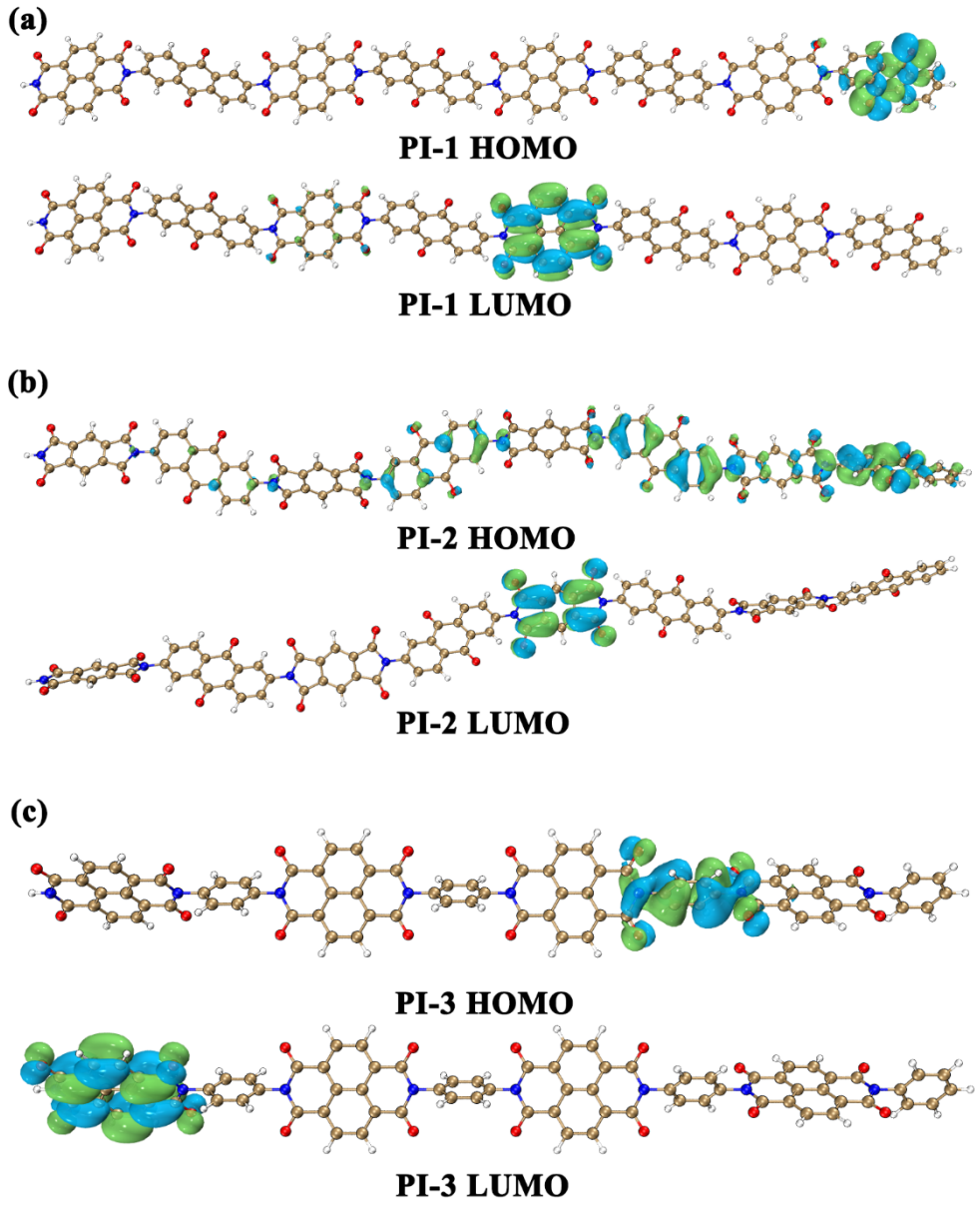

Fig. S9 Molecular orbital of the PI-1, PI-2, PI-3 (n=4).

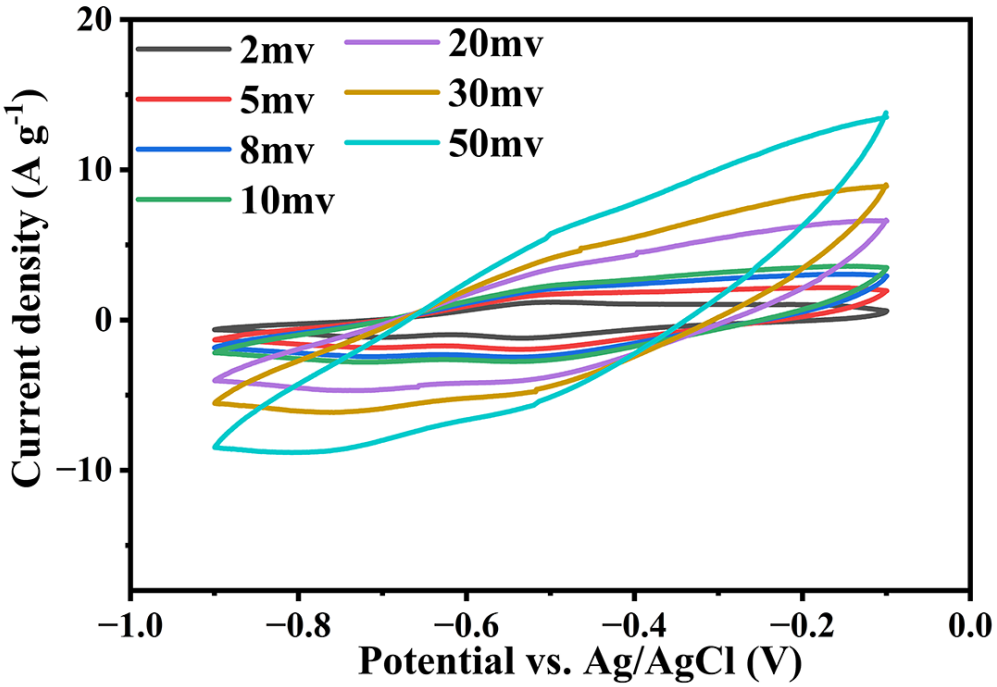

Fig. S10 CV curves of PI-1 at different scan rates.

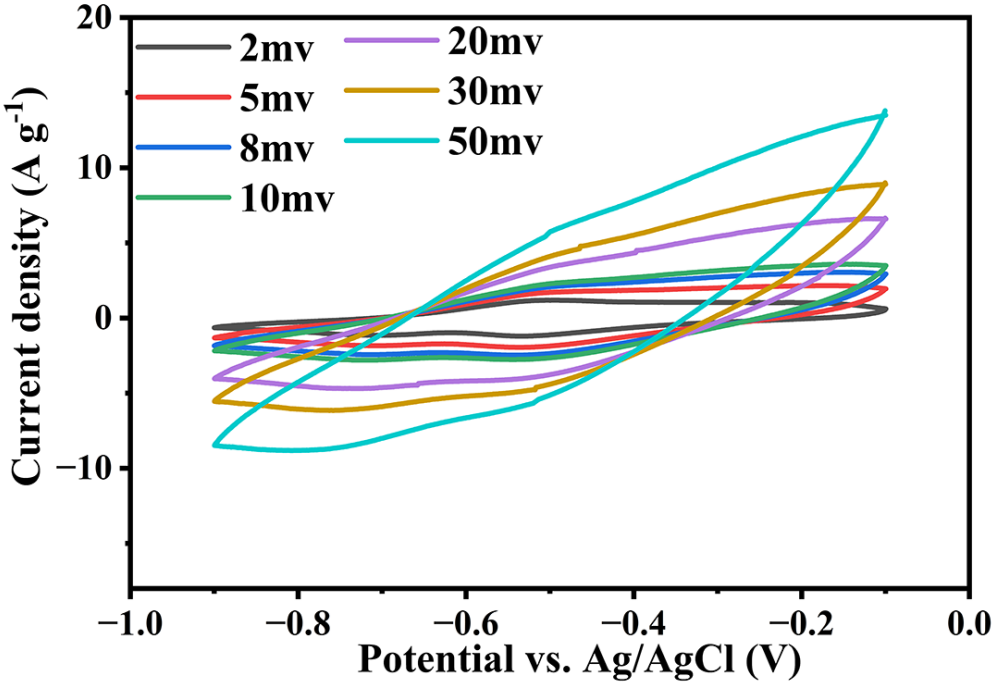

Fig. S11 CV curves of PI-2 at different scan rates.

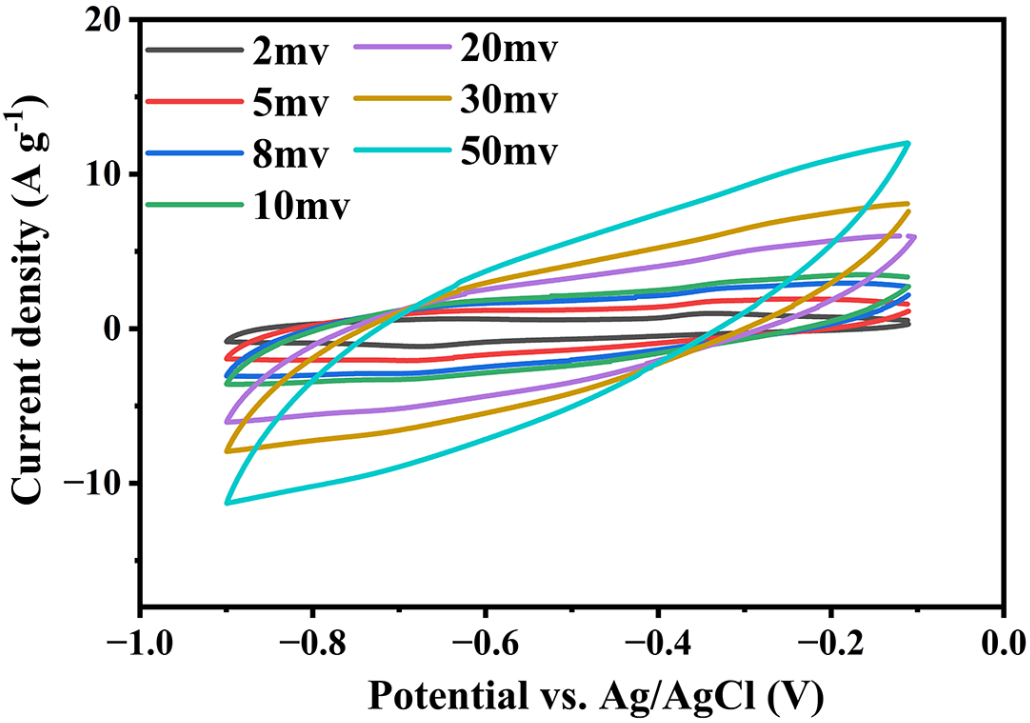

Fig. S12 CV curves of PI-3 at different scan rates.

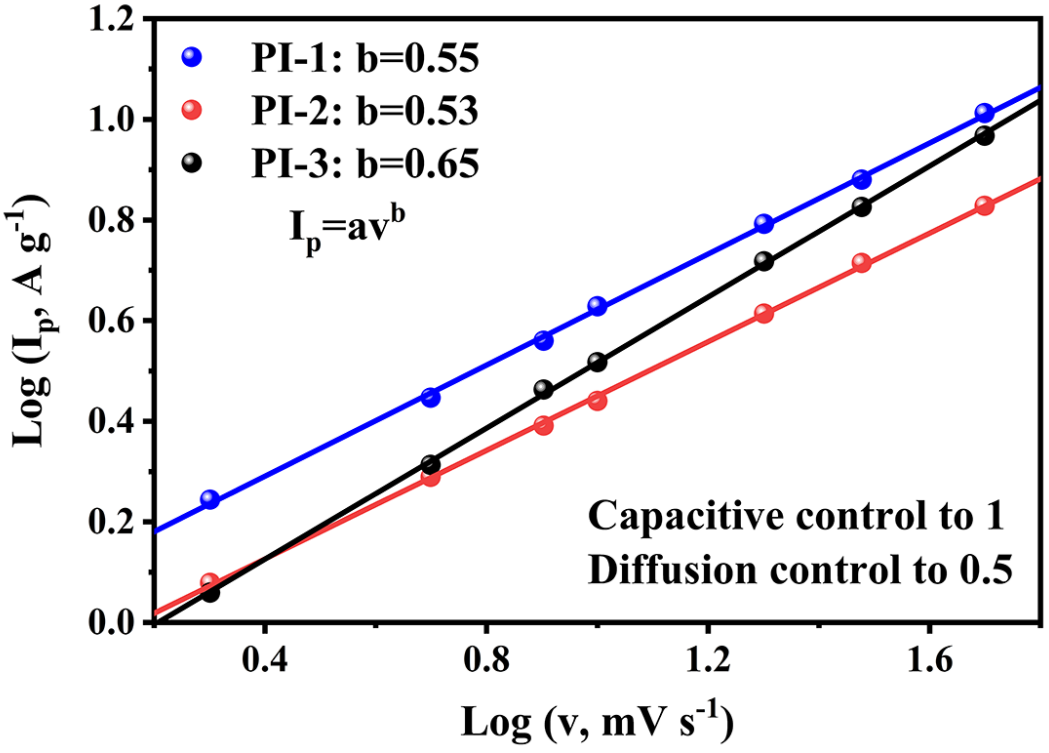

Fig. S13 The log i^{-1} vs log v of PIs.

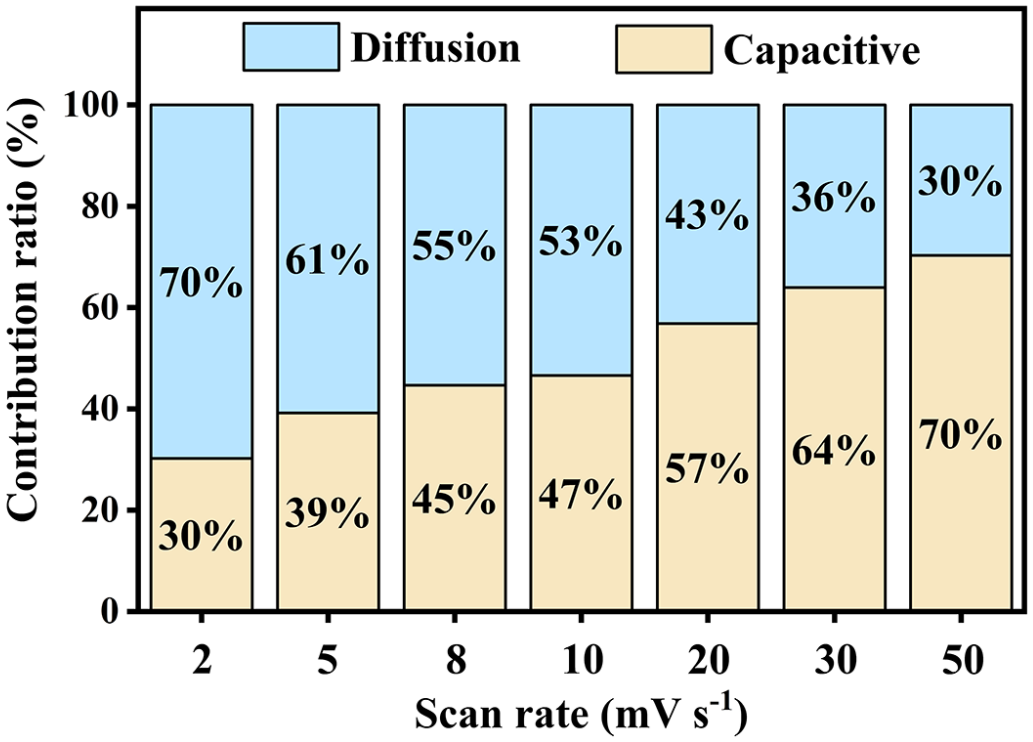

Fig. S14 Capacitive contribution of PI-1 at different scan rates.

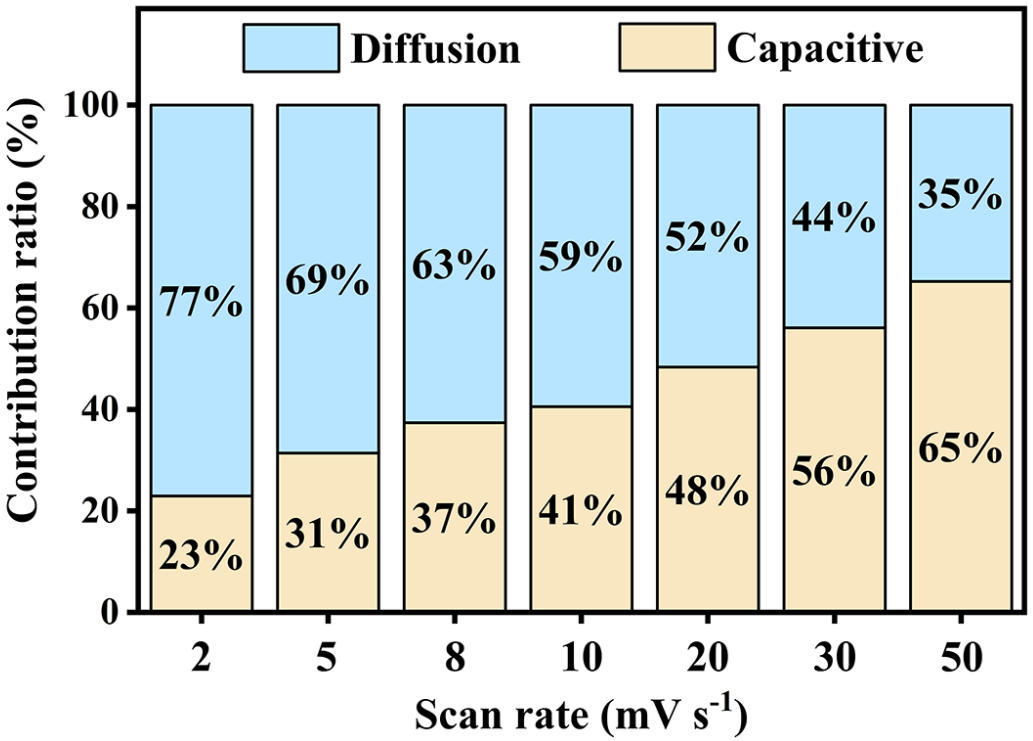

Fig. S15 Capacitive contribution of PI-2 at different scan rates.

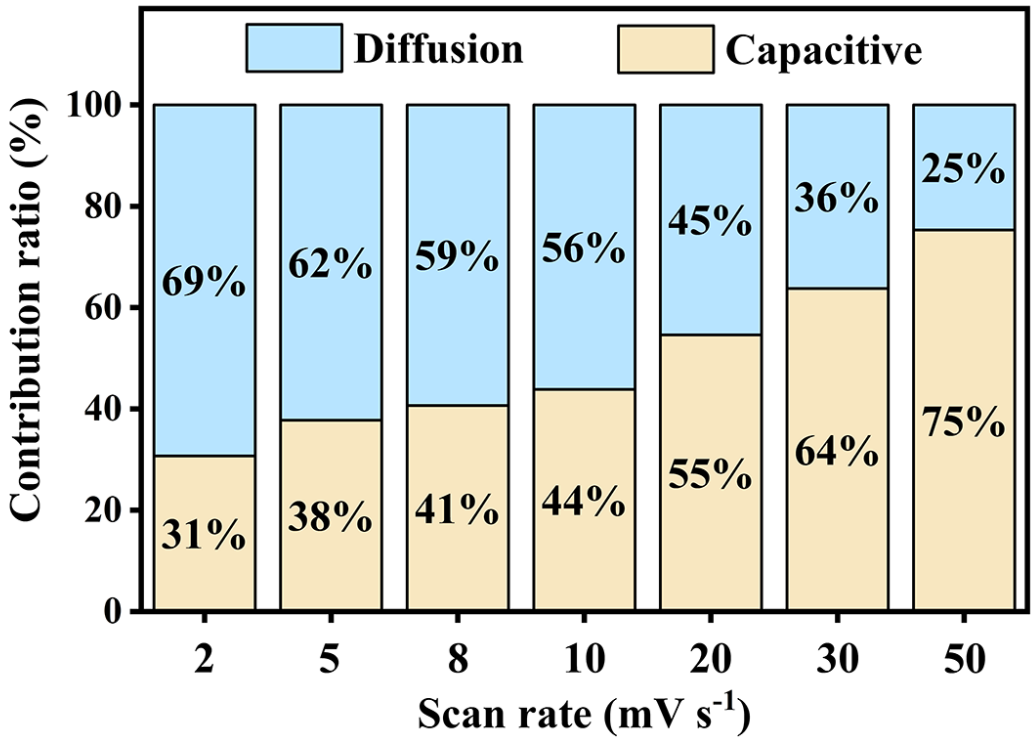

Fig. S16 Capacitive contribution of PI-3 at different scan rates.

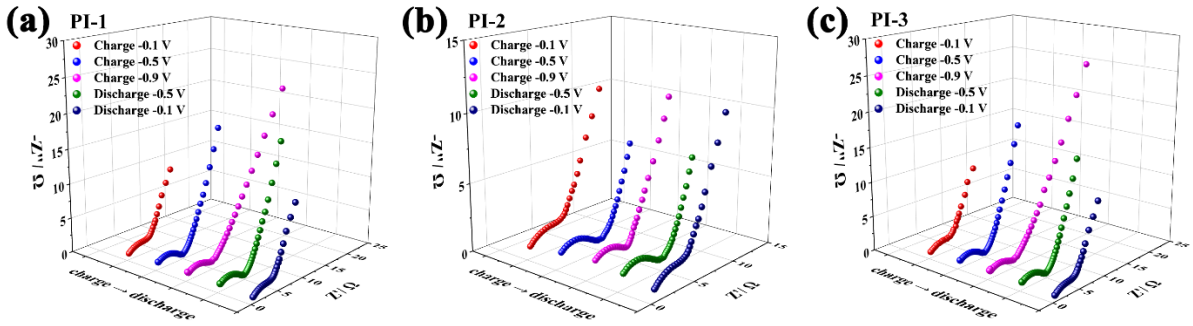

Fig. S17 Staircase-potential electrochemical impedance spectroscopy of PIs at various charged and discharged states.

Table S1 The obtained equivalent series resistance (R_s), charge transfer resistance (R_{ct}) and Warburg impedance (Z_w) of the PIs during the discharge/charge process from equivalent circuit fitting of EIS results.

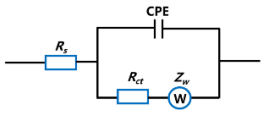	R_s (Ω)	R_{ct} (Ω)	Z_w (Ω)
Charge -0.1 V of PI-1	0.83	1.55	0.88
Charge -0.5 V of PI-1	1.16	1.73	0.80
Charge -0.9 V of PI-1	1.02	1.77	0.77
Discharge -0.5 V of PI-1	1.08	1.61	0.74
Discharge -0.1 V of PI-1	0.96	1.79	1.01
Charge -0.1 V of PI-2	1.04	2.21	1.45
Charge -0.5 V of PI-2	1.33	2.33	1.5
Charge -0.9 V of PI-2	1.40	2.33	1.50
Discharge -0.5 V of PI-2	1.36	2.37	1.54
Discharge -0.1 V of PI-2	1.06	2.24	1.47
Charge -0.1 V of PI-3	0.57	1.21	0.71
Charge -0.5 V of PI-3	0.58	1.21	0.53
Charge -0.9 V of PI-3	0.67	1.42	0.69
Discharge -0.5 V of PI-3	0.61	1.28	0.56
Discharge -0.1 V of PI-3	0.52	1.11	0.65

Staircase-potential electrochemical impedance spectroscopy (EIS, Fig. S17) provides detailed insights into the redox reaction kinetics of these PI electrodes. The corresponding equivalent circuit model and derived fitting parameters are summarized in Table S1. All Nyquist plots of three PI electrodes show no significant variation in the prominent low-frequency semicircles (corresponding to charge transfer resistance, Rct) during the charge-discharge process, indicating no obvious polarization resistance. All three PI electrodes exhibit distinct ~45° lines in the high-frequency region, demonstrating that their overall electrochemistry kinetics are dominated by ion diffusion rather than capacitive. Additionally, the order of Rct values is consistent with that of their HOMO–LUMO gaps, confirming that PIs with lower energy levels facilitate smaller charge transfer resistance.

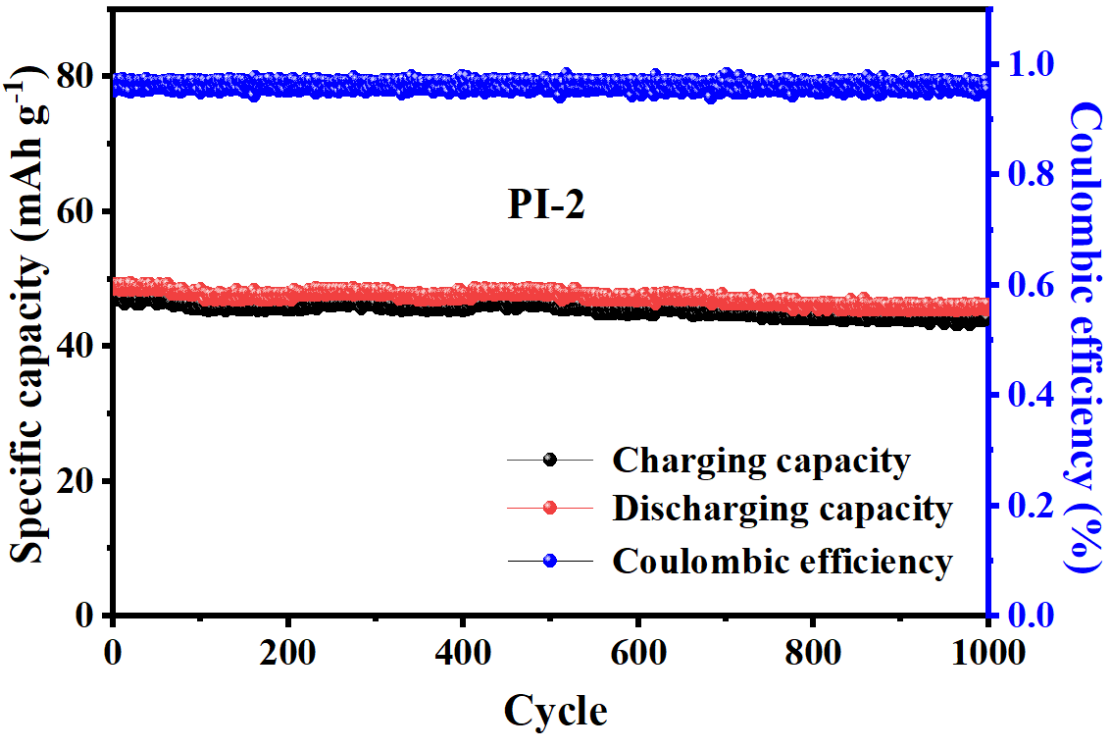

Fig. S18 GCD cycling of PI-2 electrode.

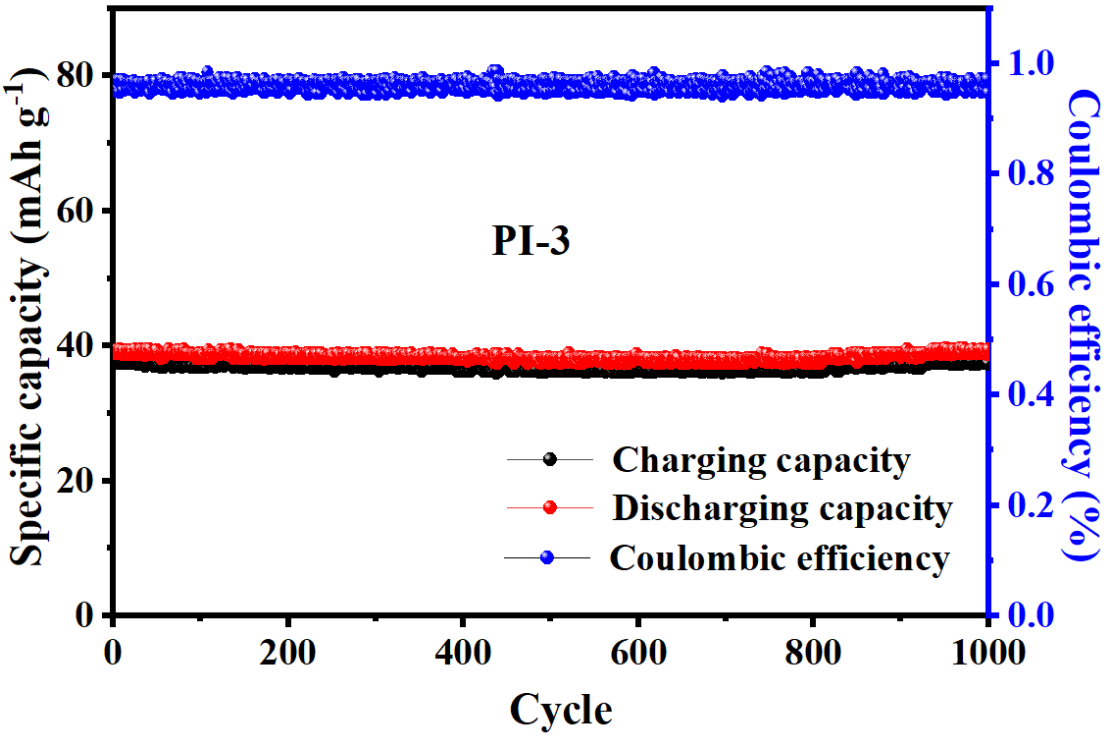

Fig. S19 GCD cycling of PI-3 electrode.

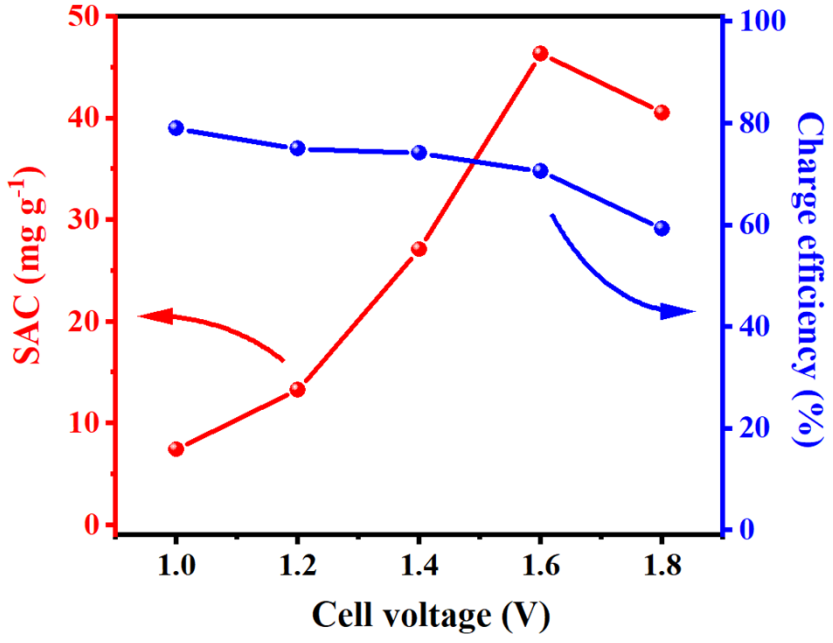

Fig. S20 Efficiency comparison of HCDI based on PI-1 cathode with different cell voltages.

The parasitic reactions at the cathode (oxygen reduction reaction and hydrogen evolution reaction) are minimized due to the deair operation before HCDI tests and the intrinsic HER-inertness of the PI electrode[8]. Therefore, the decline in charge efficiency at elevated cell-voltages (Fig. S20) is primarily attributed to carbon oxidation and minor oxygen evolution reaction on AC anode.

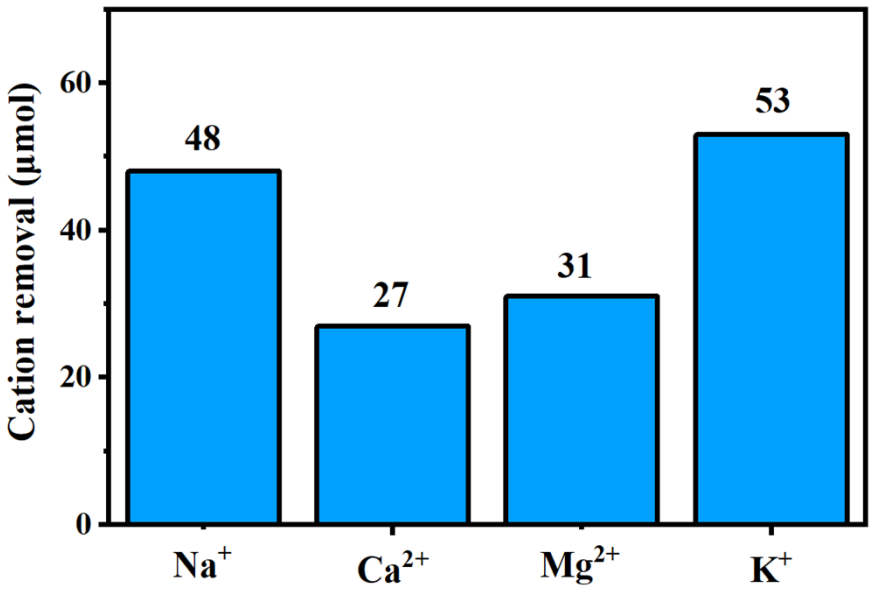

Fig. S21 Desalination performance of the HCDI based on PI-1 cathode in 80 mL mix solution (the initial concentrations of Na^+, Ca^{2+}, Mg^{2+}, and K^+ were all set to 5 mM).

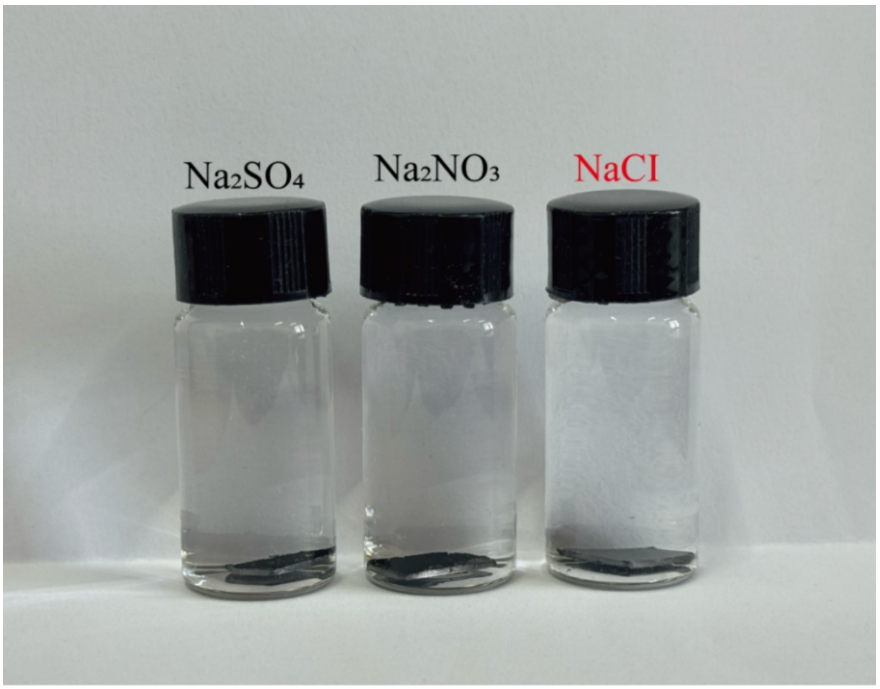

Fig. S22 Digital photo of the PI-1 electrodes soaked in different aqueous electrolytes without any dissolution after 2 weeks.

To evaluate its anti-dissolution behavior, the PI-1 electrodes were immersed in various aqueous electrolytes for 2 weeks. As shown in Fig. S22, the PI-1 electrode remains structurally intact after such treating, further confirming its excellent anti-dissolution stability in aqueous media.

References:

1. R. Wang, J. Liang, K. Zhao, D. Zhu, L. Cui, M. Wang, X. Chen, S. Zhu, Q. An and L. Zhang, *Small*, 2025, **21**, 2501631.
2. A. G. Baboul, L. A. Curtiss, P. C. Redfern and K. Raghavachari, *The Journal of chemical physics*, 1999, **110**, 7650-7657.
3. T. Lu and F. Chen, *Journal of computational chemistry*, 2012, **33**, 580-592.
4. H. William, *Journal of molecular graphics*, 1996, **14**, 33-38.
5. H. Li, L. Pan, C. Nie, Y. Liu and Z. Sun, *Journal of Materials Chemistry*, 2012, **22**, 15556-15561.
6. X. Xu, Z. Sun, D. H. Chua and L. Pan, *Scientific reports*, 2015, **5**, 11225.
7. R. Zhao, P. Biesheuvel, H. Miedema, H. Bruning and A. Van der Wal, *The Journal of Physical Chemistry Letters*, 2009, **1**, 205-210.

8. Y. Wang, X. Cui, Y. Zhang, L. Zhang, X. Gong and G. Zheng, *Advanced Materials (Deerfield Beach, Fla.)*, 2016, **28**, 7626-7632.